

Supporting information for

**Expanding the conjugated benzene rings of phenothiazine phosphonic acid for efficient tin-lead mixed perovskite solar cells with a specific Sn/Pb ratio of 0.4:0.6**

Gangsen Su,<sup>†a</sup> Qiang Sun,<sup>†a</sup> Dong He,<sup>a</sup> Tianle Cheng,<sup>a</sup> Haojie Chen,<sup>a</sup> Yuchen Pan,<sup>a</sup>  
Jinfeng Huang,<sup>a</sup> Siyuan Tang<sup>a</sup> and Zhubing He,<sup>\*ab</sup>

<sup>a</sup> Department of Materials Science and Engineering, Shenzhen Key Laboratory of Full Spectral Solar Electricity Generation (FSSEG), Southern University of Science and Technology (SUSTech), No. 1088, Xueyuan Rd, Shenzhen, 518055, Guangdong, China.

<sup>b</sup> Guangdong Provincial Key Laboratory of Sustainable Biomimetic Materials and Green Energy, Southern University of Science and Technology, Shenzhen 518055, China.

\*Corresponding author. Email: hezb@sustech.edu.cn

## Experimental Section

### Materials

Anhydrous solvents, including N,N-dimethylformamide (DMF), dimethyl sulfoxide (DMSO), chlorobenzene (CB), and isopropanol (IPA), were obtained from Sigma-Aldrich. Lead iodide (PbI<sub>2</sub>, 99.99%), 2,2-Dinaphthylamine (DNP, 98%), Ammonium thiocyanate (NH<sub>4</sub>SCN, 98%) and ethylenediamine dihydroiodide (EDAI<sub>2</sub>, 99.99%) were sourced from TCI. (4-(10H-phenothiazin-10-yl)butyl)phosphonic acid (PTZPA, 98%) was purchased from Lumtec. Tetrahydrofuran (THF, 99%), Petroleum ether (PE, 98%), dichloromethane (DCM, 98%) and 1,4-dibromobutane (DBB, 98%) were got by Energy Chemical Co., Ltd. 1,2-dichlorobenzene (99%), Potassium tert-butoxide (t-BuOK, 99%), 1,4-dioxane (99.8%), methanol (99.8%) and Methyl sulfoxide-d<sub>6</sub> were purchased from J&k Scientific. Triethyl phosphite (98%) and Sulfur (99.99%) were purchased from Aladdin. Trimethyl bromosilane (98%) were purchased from Adamas-beta. Formamidinium iodide (FAI, 99.99%) and methylammonium iodide (MAI, 99.99%) were acquired from Great Cell Solar. Bathocuproine (BCP, >99%), phenyl-C<sub>61</sub>-butyric acid methyl ester (PC<sub>61</sub>BM, >99%), and PEDOT:PSS were purchased from Xi'an Yuri Solar Co., Ltd. Silver (Ag) and tin fluoride (SnF<sub>2</sub>) were sourced from Sigma-Aldrich, while tin iodide (SnI<sub>2</sub>) was provided by 3AChem. Fullerene (C<sub>60</sub>) was purchased from Liaoning Youxuan New Energy Technology Co., Ltd. ITO glass from Suzhou ShangYang Solar Technology Co., Ltd.

### Device fabrication

The inverted (p-i-n) PSCs examined in this study features an architecture of ITO/HTL/Perovskite/EDAI<sub>2</sub>/PC<sub>61</sub>BM/C<sub>60</sub>/BCP/Ag. To prepare the perovskite precursor solution, 4.9 mg of NH<sub>4</sub>SCN, 10.7 mg of SnF<sub>2</sub>, 95.4 mg of MAI, 240.8 mg of FAI, 553.2 mg of PbI<sub>2</sub>, and 298 mg of SnI<sub>2</sub> were dissolved in 1050 μL of a DMF and DMSO mixture (volume ratio 750:300) stirred for 12 hours. To prepare the passivation solution, 0.5 mg of EDAI<sub>2</sub> was dissolved in 1 mL of a 995:5 volume ratio of IPA and

DMF stirred for 6 hours at 60 °C. The fabrication process began with cleaning the ITO glass substrate in an ultrasonic bath, sequentially using detergent in water, deionized water, acetone, and isopropanol, each for 20 minutes. The cleaned substrate was then dried with N<sub>2</sub> gas and subjected to UV-ozone treatment for 30 minutes. The PEDOT:PSS dispersion was spin-coated onto the ITO substrate and annealed at 150 °C for 10 minutes. Subsequently, the substrates were transferred into an N<sub>2</sub>-filled glovebox. An 80 µL 0.5 mg/ml solution of PTZPA/DB-PTZPA in THF was spin-coated onto cleaned ITO substrates at 4000 rpm for 35 seconds, followed by annealing at 100 °C for 10 min at the N<sub>2</sub>-filled glovebox. The prepared perovskite precursor solution was spin-coated onto the PEDOT:PSS, PTZPA or DB-PTZPA layer, initially at 1000 rpm for 10 seconds, then at 4000 rpm for 60 seconds. During the final 35 seconds, 500 µL of chlorobenzene was drop-cast onto the spinning film, which was then annealed at 100 °C for 10 minutes. The EDAl<sub>2</sub> solution was static spin-coated onto the perovskite layer at 4000 rpm for 35 seconds, followed by annealing at 80 °C for 5 minutes. A layer of PC<sub>61</sub>BM (3 mg/mL in chlorobenzene) was then spin-coated at 6000 rpm for 35 seconds and annealed at 80 °C for 1 min. This was followed by the thermal evaporation of an 18 nm layer of C<sub>60</sub> and a 7 nm layer of BCP. Finally, a 100 nm thick layer of Ag was deposited via thermal evaporation to complete the device structure.

### **Characterizations**

Ultraviolet photoelectron spectroscopy (UPS) spectra, used to measure the work function, were recorded on an Imaging Photoelectron Spectrometer (Axis Ultra, Kratos Analytical Ltd) with a non-mono chromated He I $\alpha$  photon source ( $h\nu = 21.22$  eV), using Au as a reference. Scanning electron microscopy (SEM) images were obtained using a HITACHI SU8230. FTIR spectra were recorded on a Bruker Vertex 70v. The surface roughness, current and potential were tested using an MFP-3D-Stand Alone Atomic Force Microscope (AFM, Oxford Instrument). UV-vis spectra were obtained on a PerkinElmer Lambda 950 spectrometer. X-ray diffraction (XRD) spectra were measured by Bruker D8 ADVANCE. The NMR spectra were recorded using Bruker Advance 500 and Bruker Advance 400 spectrometers in DMSO-d<sub>6</sub>.

**Device performance characterization:**

All photovoltaic characterizations were conducted under ambient conditions (~20 °C, ~60% RH). Current density-voltage ( $J$ - $V$ ) curves were acquired using a Keithley 2400 source meter with a 200 ms delay per data point, scanning bidirectionally: reverse (0.9 V to 0.2 V) and forward (-0.2 V to 0.9 V) at 0.01 V increments. A shadow mask defined the 0.08 cm<sup>2</sup> active area during testing. The AM 1.5G spectrum was generated by an Oriel Sol3A solar simulator, calibrated to 100 mW/cm<sup>2</sup> irradiance via a KG-5 silicon reference cell. Electrochemical impedance spectroscopy (EIS) and Mott-Schottky analyses employed a Zahner Zennium workstation. External quantum efficiency (EQE) spectra utilized an EnliTech system with wavelength-specific calibration through a monocrystalline Si reference. Stabilized power output (SPO) tracking maintained bias at  $V_{max}$  under continuous illumination without thermal regulation. For operational stability assessment, encapsulated devices underwent 1 sun equivalent LED aging (ambient conditions), with maximum power point logged at 1 min intervals.

**DFT calculation**

The DFT calculations were performed with the Gaussian 09 revision D.01 suite. Electrostatic potential profiles, molecular frontier orbitals, and molecular geometry of PTZPA were calculated by the B3LYP and 6-31+G(d) basis set with vdW dispersion-corrected functionals 7 (DFT-D3). Through the calculation of vibration frequency, the optimized molecular structure had no virtual frequency.

### Synthesis of DBP

In a 100 mL Schlenk tube, 2.0 g (7.42 mmol) of DNP, 475 mg (14.84 mmol) of elemental sulfur, and 56.6 mg (0.22 mmol) of iodine were added. The system was purged with N<sub>2</sub> three times to remove oxygen. Then, 20 mL of anhydrous 1,2-dichlorobenzene was introduced as the solvent. The reaction mixture was heated to 160 °C and maintained at this temperature for 6 hours. Upon completion of the reaction, the product was purified by flash chromatography using dichloromethane as the eluent, and the organic phase was collected. The solvent was removed under reduced pressure using a rotary evaporator, yielding an orange-yellow solid. The crude product was recrystallized from dichloromethane, and the yellow solid product (2.1 g, yield 93.85%) was obtained after filtration.

<sup>1</sup>H NMR (400 MHz, DMSO-d<sub>6</sub>) δ 9.06 (s, 1H), 7.94–7.80 (m, 4H), 7.70 (d, J = 8.0 Hz, 1H), 7.68 (d, J = 8.0 Hz, 1H), 7.58 (dd, J = 7.5, 1.0 Hz, 1H), 7.55–7.34 (m, 4H), 7.11–7.09 (m, 2H) ppm.

<sup>13</sup>C NMR (101 MHz, DMSO-d<sub>6</sub>) δ 140.81, 130.52, 130.40, 128.87, 128.24, 127.64, 123.95, 122.02, 117.25, 107.41 ppm.

### Synthesis of DB-PTZC4Br

A 100 mL Schlenk tube was charged with DBP (2.0 g, 6.64 mmol) and t-BuOK (2.99 g, 26.56 mmol). The system was purged with N<sub>2</sub> three times, after which 40 mL of anhydrous THF was added, and the mixture was stirred for 1 hour. A separate 100 mL two-necked flask was charged with 10 mL of anhydrous THF and 10 mL of 1,4-dibromobutane, and the system was purged with nitrogen three times before being placed in an ice bath. The mixture of DBP and t-BuOK was then added dropwise to the flask containing anhydrous THF and 1,4-dibromobutane. The reaction was allowed to proceed at room temperature for 12 hours. Upon completion of the reaction, deionized water was added to quench the reaction, and the mixture was extracted three times with dichloromethane. The combined organic phases were dried over anhydrous magnesium sulfate, and the solvent was removed under reduced pressure using a rotary evaporator. The concentrated organic phase was purified by column chromatography using a petroleum ether/dichloromethane (8:1, v/v) mixture as the eluent. The final product, DB-PTZC4Br, was obtained as a yellow solid (1.4 g, 48.6% yield).

<sup>1</sup>H NMR (400 MHz, DMSO-d<sub>6</sub>) δ 8.23–7.84 (m, 6H), 7.61–7.41 (m, 6H), 4.23–4.20 (m, 2H), 3.53–3.50 (m, 3H), 2.01–1.82 (m, 6H) ppm.

<sup>13</sup>C NMR (101 MHz, DMSO-d<sub>6</sub>) δ 144.54, 131.16, 130.40, 128.69, 128.21, 127.66, 124.88, 122.77, 117.97, 117.38, 47.00, 35.28, 30.03, 26.95 ppm.

### Synthesis of DB-PTZPA

DB-PTZC4Br (1.4 g, 3.23 mmol) and triethyl phosphite (20 mL) were added to a 100 mL Schlenk tube, then the mixture was heated to 160 °C and stirred overnight under N<sub>2</sub>. Excess triethyl phosphite was removed by distillation under reduced pressure to give a pale yellow oil which did not require further purification. The oil was dissolved in anhydrous 1,4-dioxane (15 mL) at room temperature, trimethyl bromosilane (4.94 g,

32.3 mmol) was added dropwise and the mixture was stirred for 24 h. Subsequently, 15 mL of methanol was added and stirred for 3 h. Deionized water was then added dropwise until the mixture became opaque, and then the mixture was stirred for 12 h. The mixture was then stirred for 12 h. The crude product was dissolved in a mixture of 1,4-dioxane (15 mL) and trimethyl bromosilane (4.94 g, 32.3 mmol). The crude product was dissolved in THF (5 mL), precipitated in petroleum ether (20 mL) and filtered, repeated twice to give a yellow-green solid (0.70 g, 50% yield).

**<sup>1</sup>H NMR** (400 MHz, DMSO-d<sub>6</sub>) δ 8.23 – 7.83 (m, 6H), 7.60 – 7.40 (m, 5H), 4.18 – 4.15 (m, 3H), 2.50 – 2.48 (m, 5H), 1.85 – 1.45 (m, 10H) ppm.

**<sup>13</sup>C NMR** (101 MHz, DMSO) δ 144.63, 131.16, 130.35, 128.67, 128.15, 127.63, 124.82, 122.77, 117.89, 117.15, 47.51, 29.19, 28.31, 26.95, 20.68 ppm.

**<sup>31</sup>P NMR** (243 MHz, DMSO) δ 26.46 ppm.

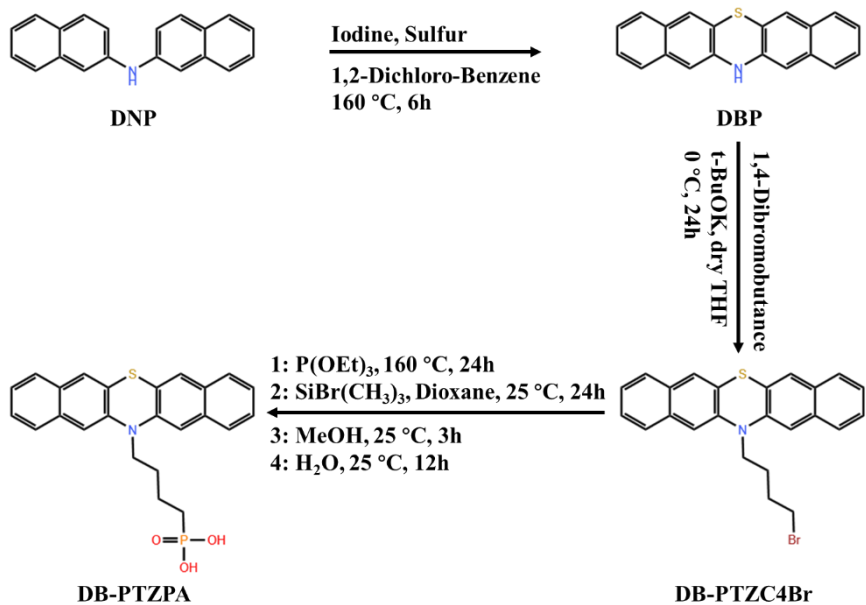


**Figure S1.** Synthetic route of DB-PTZPA.

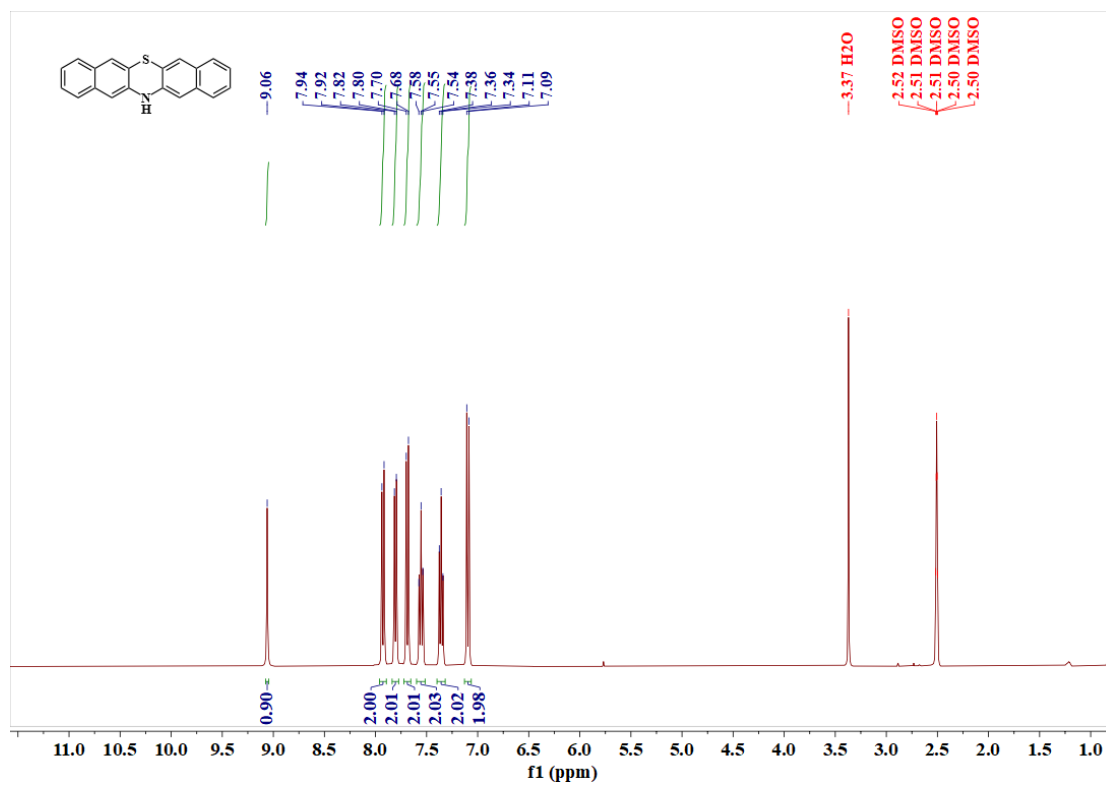


**Figure S2.** <sup>1</sup>H NMR spectrum of DBP.

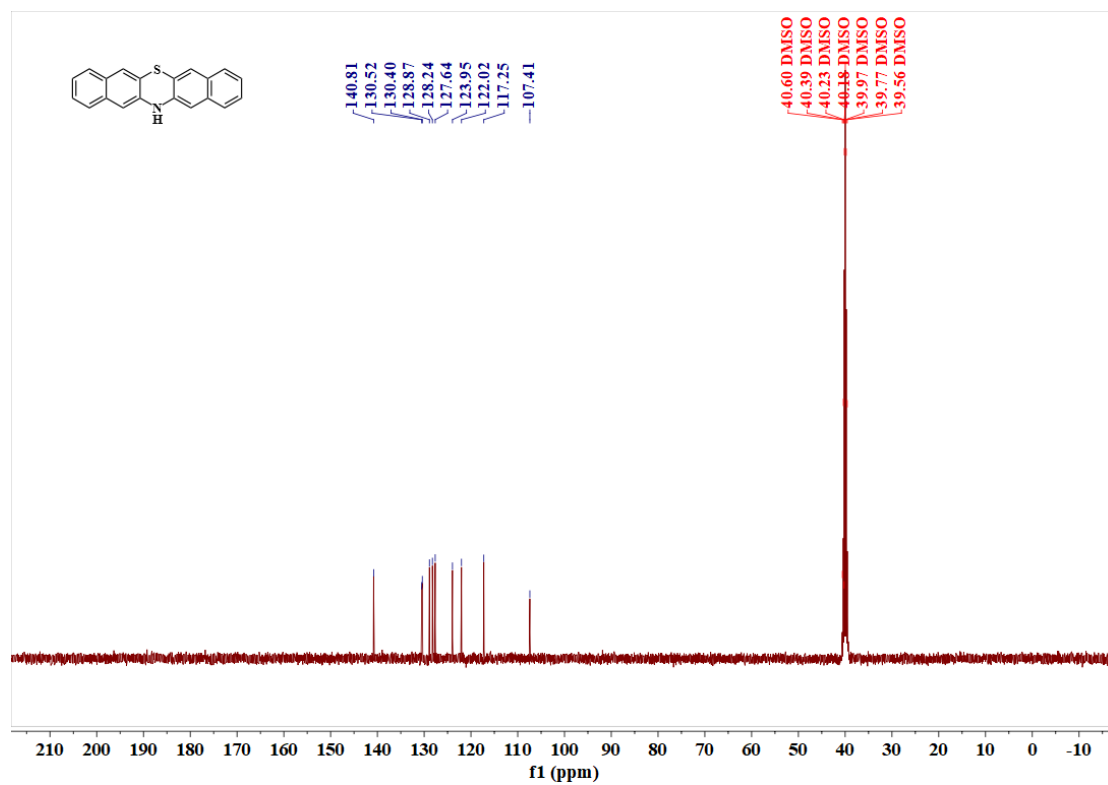


**Figure S3.**  $^{13}\text{C}$  NMR spectrum of DBP.

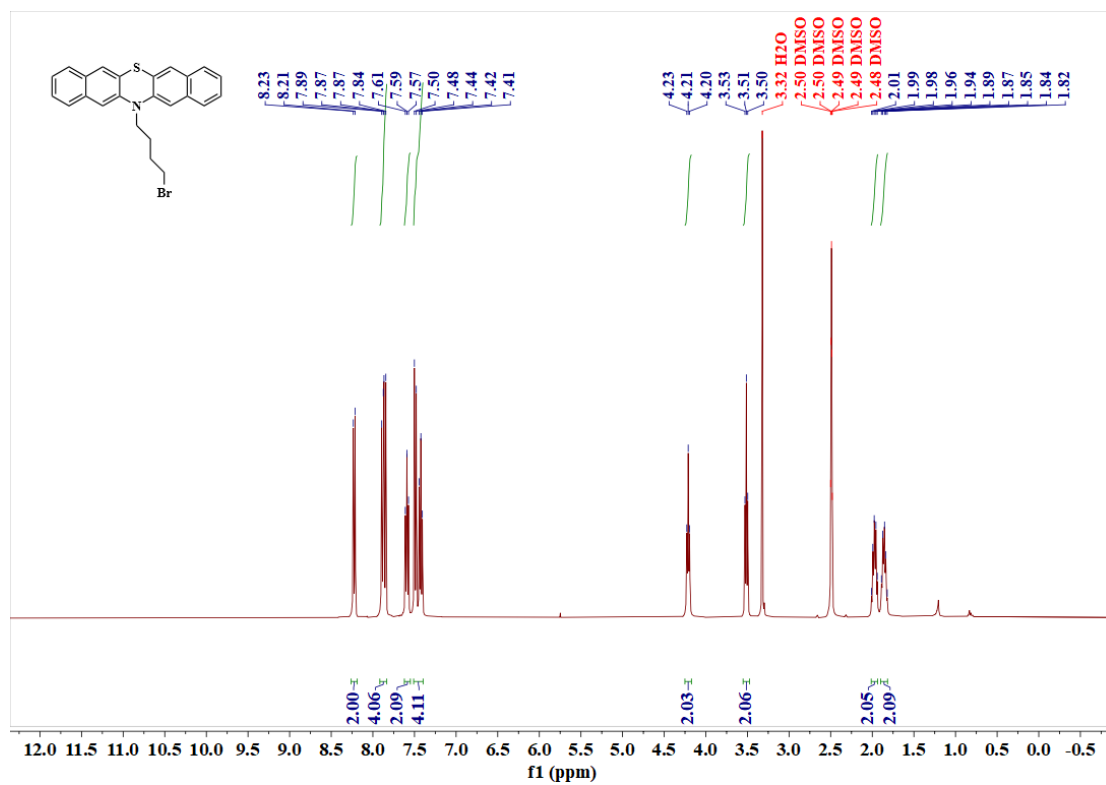


**Figure S4.** <sup>1</sup>H NMR spectrum of DB-PTZC4Br.

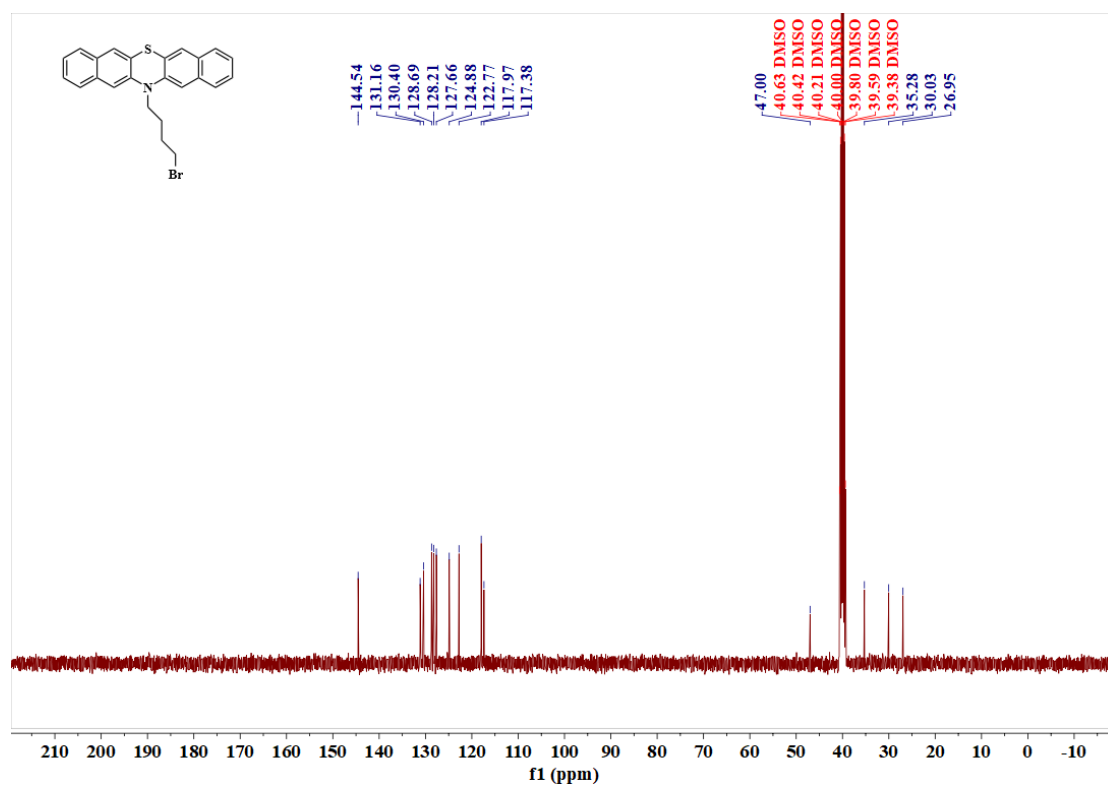


**Figure S5.**  $^{13}\text{C}$  NMR spectrum of DB-PTZC4Br.

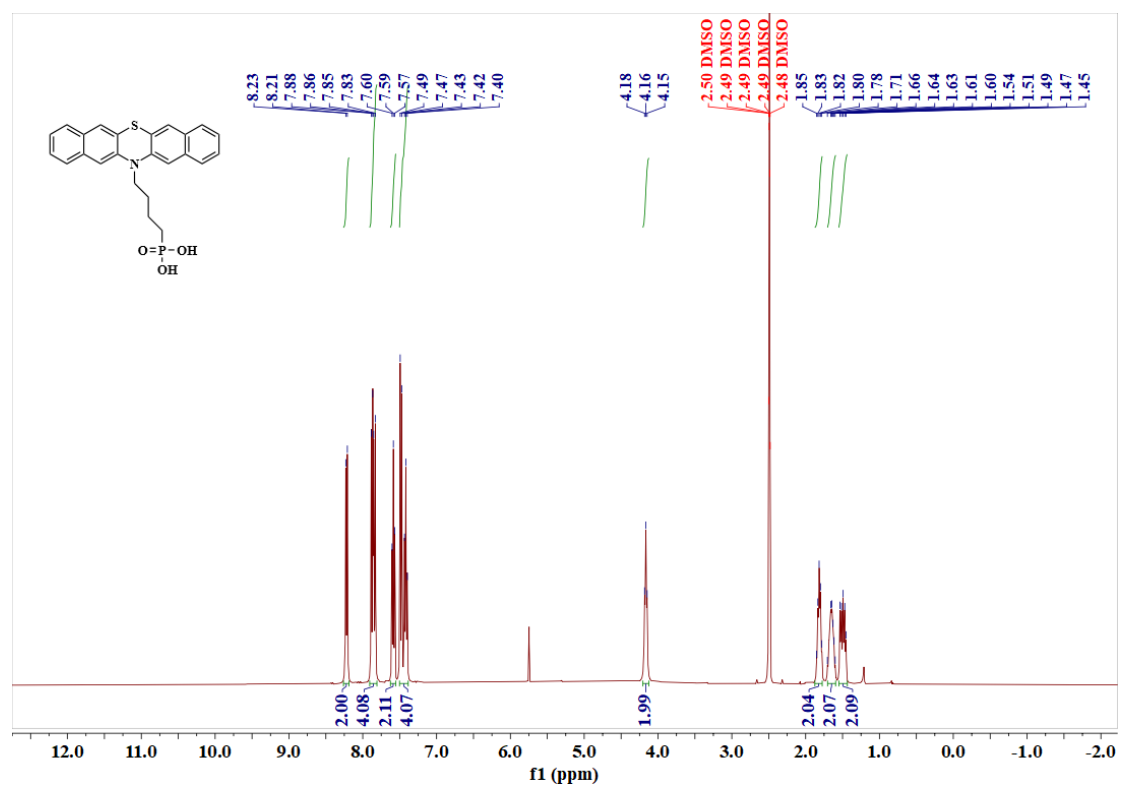


**Figure S6.** <sup>1</sup>H NMR spectrum of DB-PTZPA.

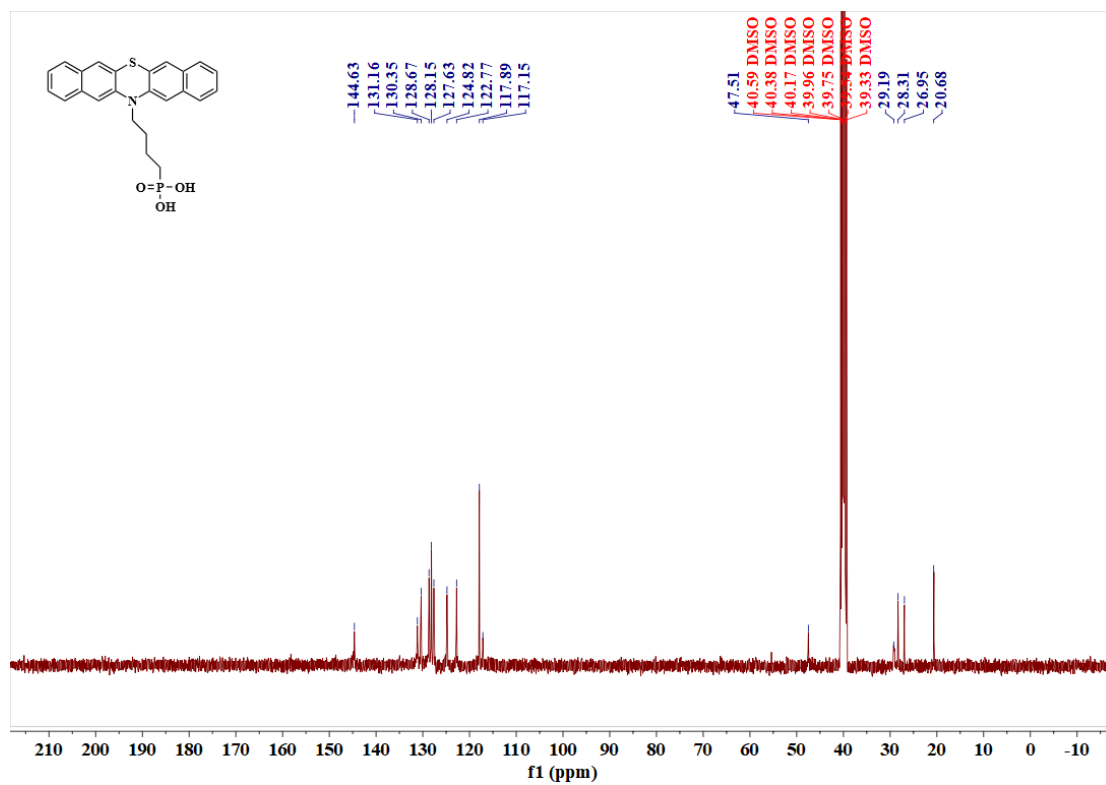


**Figure S7.** <sup>13</sup>C NMR spectrum of DB-PTZPA.

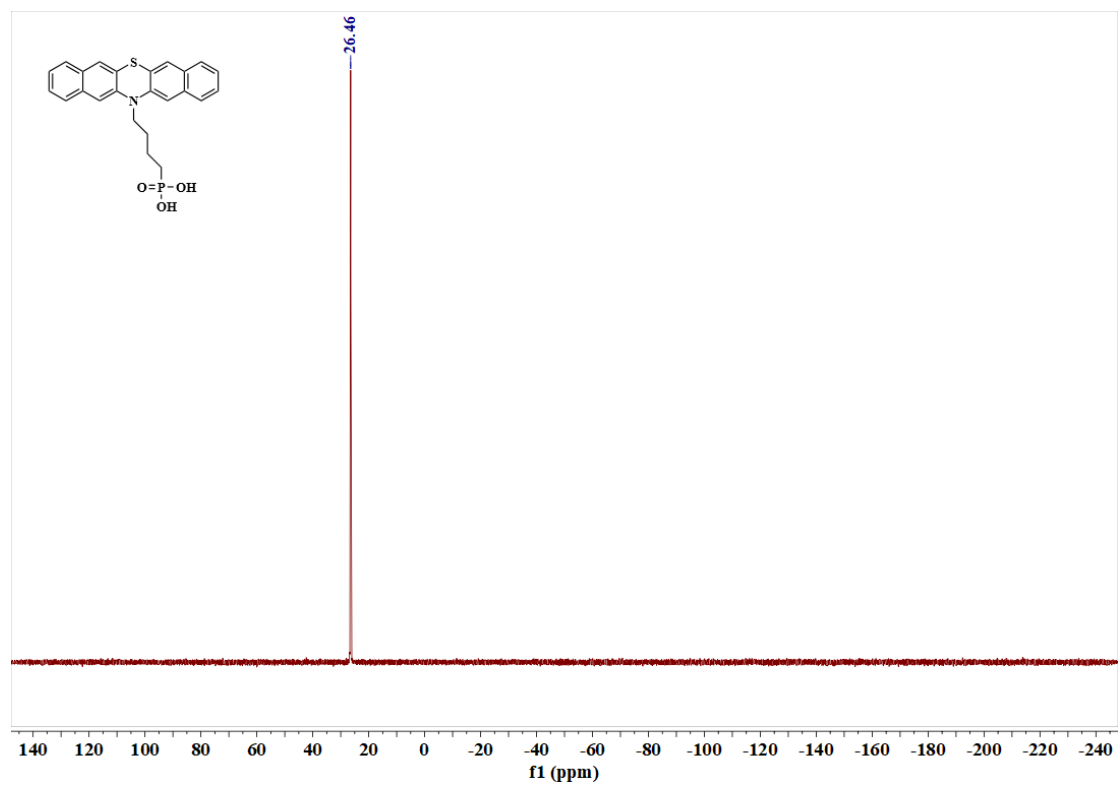


**Figure S8.**  $^{31}\text{P}$  NMR spectrum of DB-PTZPA.

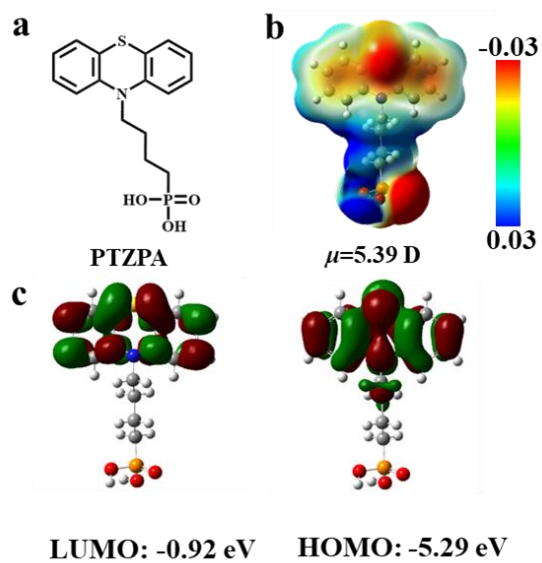


**Figure S9.** (a) Molecular structure of PTZPA. (b) Calculated ESP of PTZPA. (c) Calculated LUMO and HOMO energy levels of PTZPA.

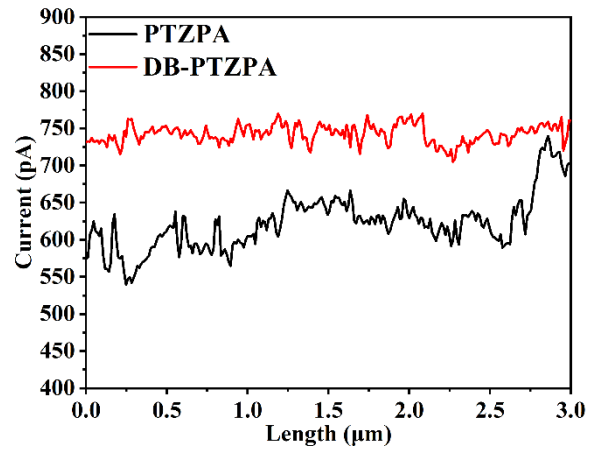


**Figure S10.** Current image of the c-AFM sectional diagram corresponding to ITO/PTZPA(DB-PTZPA).

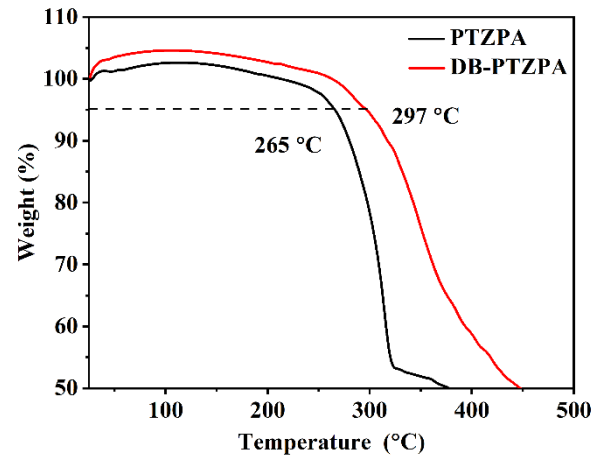


**Figure S11.** TGA of PTZPA and DB-PTZPA with a heating rate of 10 °C/min in nitrogen flow.

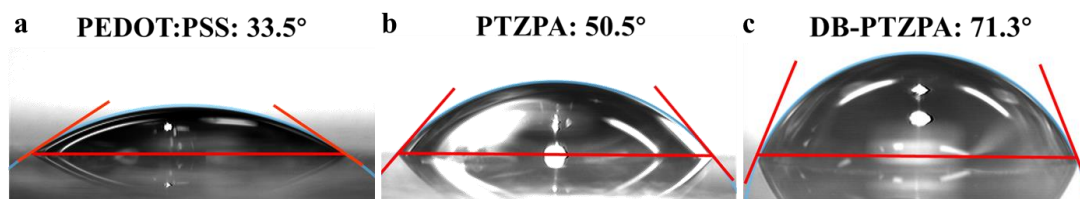


**Figure S12.** Contact angles of (a) ITO/PEDOT:PSS, (b) ITO/PTZPA, and (c) ITO/DB-PTZPA with respect to water.

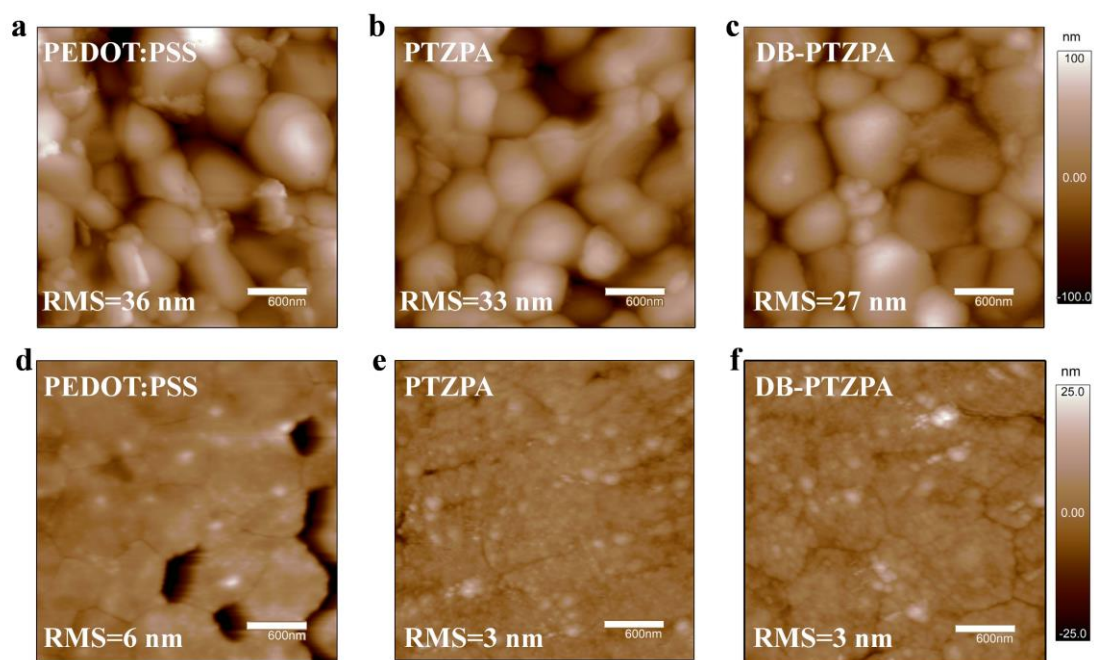


**Figure S13.** Top surfaces view of AFM images for (a) PEDOT:PSS/TLP, (b) PTZPA/TLP, and (c) DB-PTZPA/TLP. Buried interfaces view of AFM images for (d) PEDOT:PSS/TLP, (e) PTZPA/TLP, and (f) DB-PTZPA/TLP.

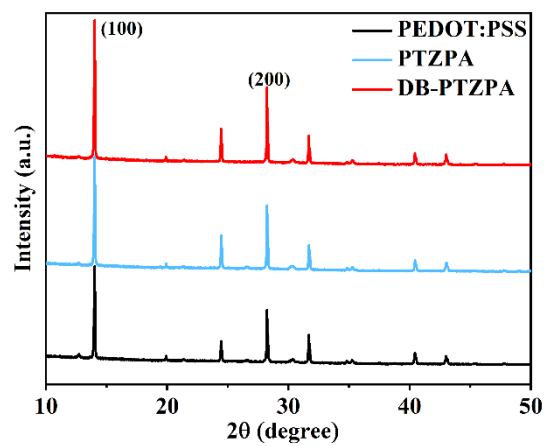


**Figure S14.** XRD of PEDOT:PSS/TLP, PTZPA/TLP and DB-PTZPA/TLP.

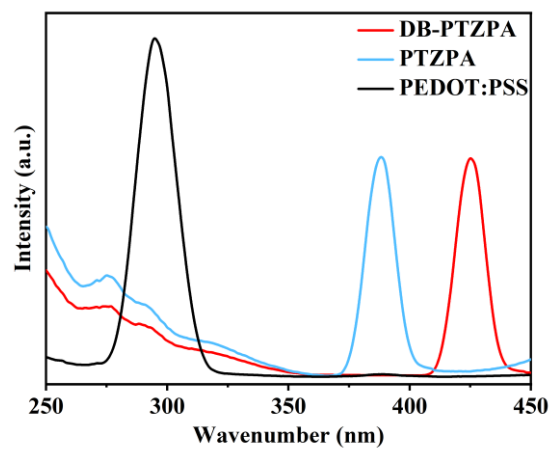


**Figure S15.** Photoluminescence of ITO/PEDOT:PSS, ITO/PTZPA and ITO/DB-PTZPA.

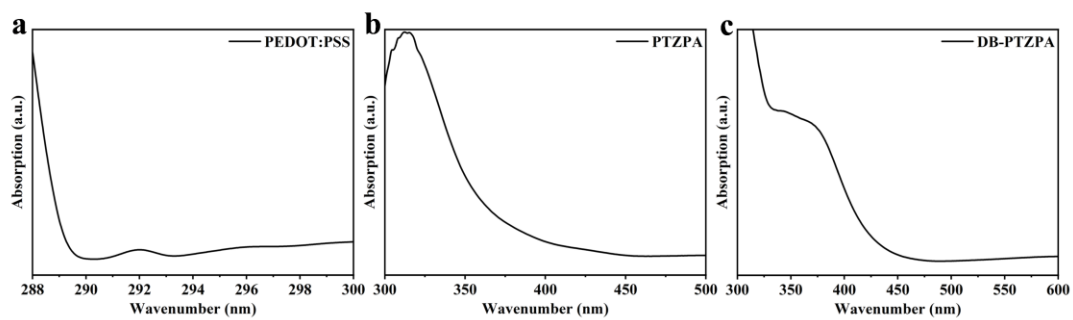


**Figure S16.** UV-vis absorption spectra of PEDOT:PSS, PTZPA, and DB-PTZPA.

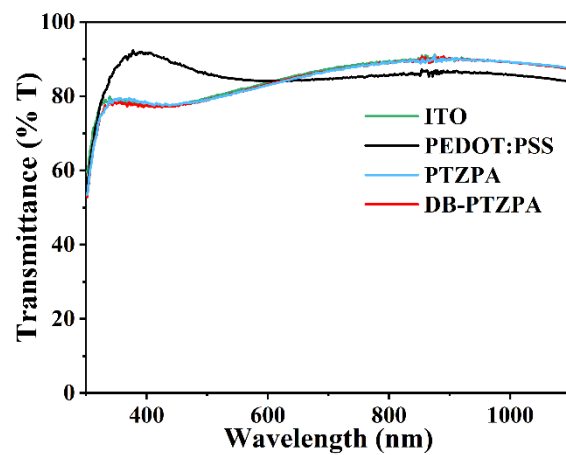


**Figure S17.** Transmission spectra of bare ITO, ITO/PEDOT:PSS, ITO/PTZPA and ITO/DB-PTZPA.

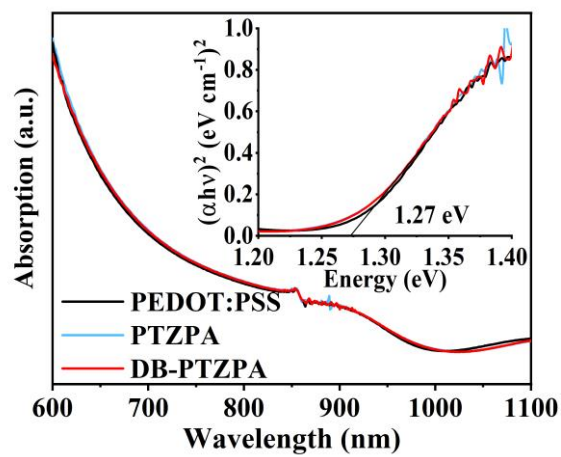


**Figure S18.** UV absorption spectrum and Tauc plot of TLP for PEDOT:PSS, PTZPA and DB-PTZPA.

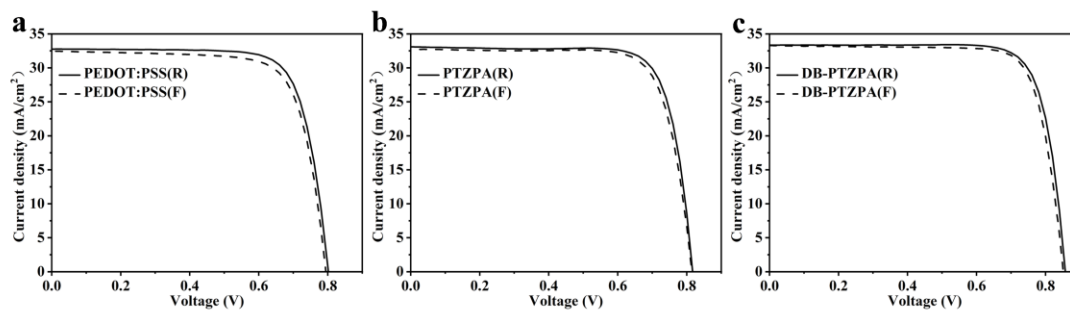


**Figure S19.** Forward and reverse sweep  $J$ - $V$  curve of PEDOT:PSS, PTZPA, and DB-PTZPA-based device.

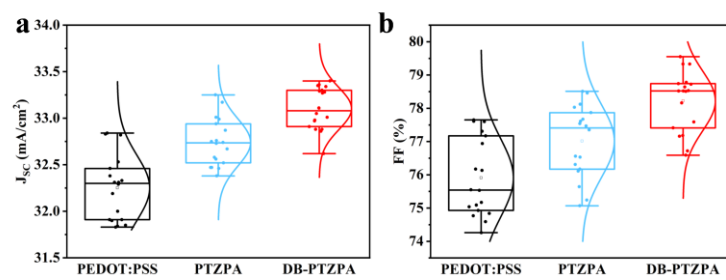


**Figure S20.** Statistics of PEDOT:PSS, PTZPA and DB-PTZPA-based TLP solar cell (a)  $J_{sc}$  and (b)  $FF$ . Each parameter was collected from a batch of 18 individual cells.

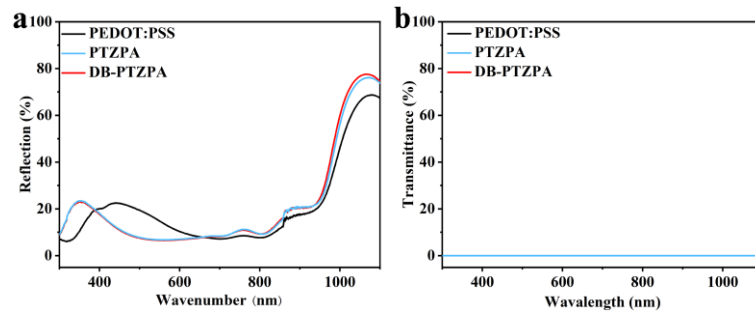


**Figure S21.** Reflection (a) and transmission (b) spectra of devices based on PEDOT:PSS, PTZPA, and DB-PTZPA-based intact solar cells.

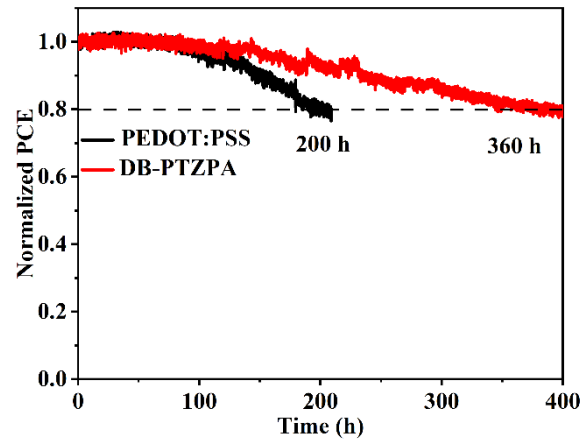


**Figure S22.** Encapsulated PEDOT:PSS and DB-PTZPA-based PSCs light soaking test in MPP mode at an ambient atmosphere. The stability of DB-PTZPA based TLP solar cell is still low and needs enhancing by improving the film quality and encapsulation.

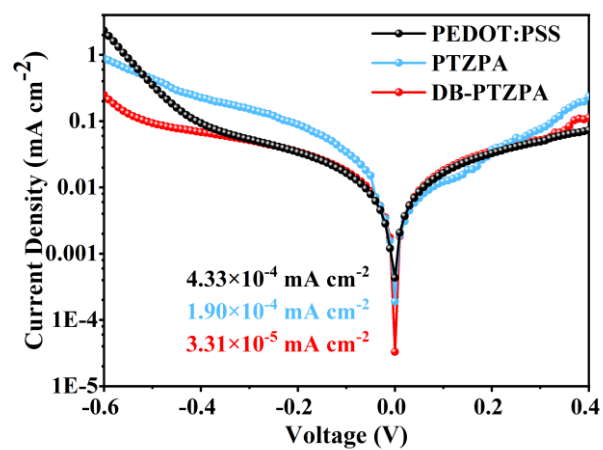


**Figure S23.** Dark current density measurements of PEDOT:PSS , PTZPA and DB-PTZPA base Sn-Pb mixed PSCs.

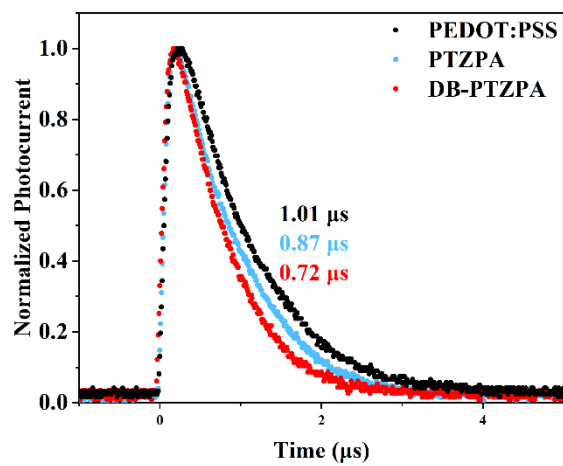


**Figure S24.** Transient photocurrent (TPC) tests of PEDOT:PSS , PTZPA and DB-PTZPA base Sn-Pb mixed PSCs.

**Table S1.** Summary of reported performance of Sn<sub>0.4</sub>Pb<sub>0.6</sub>-based TLP solar cells.

Solar cell configuration	Voc (V)	Jsc (Ma cm <sup>-2</sup> )	FF (%)	PCE (%)	Year
ITO/PEDOT:PSS/NiO <sub>x</sub> /MASn <sub>0.4</sub> Pb <sub>0.6</sub> I <sub>3</sub> / PCBM/Al	0.75	17.8	61.6	8.2	2017 <sup>1</sup>
ITO/PEDOT:PSS/(t-A) <sub>2</sub> (FA <sub>0.85</sub> Cs <sub>0.15</sub> ) <sub>n-1</sub> (Sn <sub>0.4</sub> Pb <sub>0.6</sub> ) <sub>n</sub> I <sub>3n+1</sub> /PCBM/BCP/Ag	0.7	24.2	63	10.6	2018 <sup>2</sup>
ITO/FA <sub>0.75</sub> Cs <sub>0.25</sub> Sn <sub>0.4</sub> Pb <sub>0.6</sub> I <sub>3</sub> /C <sub>60</sub> / BCP/Ag	0.7	30.22	73.07	15.35	2019 <sup>3</sup>
ITO/PEDOT:PSS/ FA <sub>0.85</sub> /MA <sub>0.15</sub> Sn <sub>0.4</sub> Pb <sub>0.6</sub> I <sub>2.55</sub> Br <sub>0.45</sub> /PCBM/C <sub>60</sub> / Ag	0.87	26.45	79.1	18.21	2019 <sup>4</sup>
FTO/TiO <sub>2</sub> /MAPb <sub>0.6</sub> Sn <sub>0.4</sub> I <sub>3</sub> /CuSCN/Ag	0.73	11.8	55	4.96	2022 <sup>5</sup>
FTO/PTAA(PFN)/FA <sub>0.83</sub> Cs <sub>0.17</sub> Sn <sub>0.4</sub> Pb <sub>0.6</sub> I <sub>3</sub> / PCBM/BCP/Ag	0.79	26.2	68	14.1	2020 <sup>6</sup>
FTO/NiO <sub>x</sub> /CsSn <sub>0.4</sub> Pb <sub>0.6</sub> I <sub>3</sub> /PCBM/BCP/Ag	0.77	25.87	66.7	13.37	2020 <sup>7</sup>
ITO/NiO <sub>x</sub> /CsSn <sub>0.4</sub> Pb <sub>0.6</sub> I <sub>2</sub> Br /ZnO/ PC <sub>61</sub> BM/Ag	0.87	22.67	71.73	14.17	2022 <sup>8</sup>
FTO/NiO <sub>x</sub> /CsSn <sub>0.4</sub> Pb <sub>0.6</sub> I <sub>3</sub> /PCBM/BCP/Ag	0.88	23.68	71.9	15.04	2022 <sup>9</sup>
ITO/TPA-HATNA/FA <sub>0.8</sub> Cs <sub>0.2</sub> Sn <sub>0.4</sub> Pb <sub>0.6</sub> I <sub>3</sub> / C <sub>60</sub> /BCP/Ag	0.79	29.04	78.69	18.05	2022 <sup>10</sup>
ITO/PEDOT:PSS/Cs <sub>0.25</sub> FA <sub>0.75</sub> Sn <sub>0.4</sub> Pb <sub>0.6</sub> I <sub>3</sub> / PCBM/BCP/Ag	0.88	30.56	80.36	21.61	2022 <sup>11</sup>
FTO/NiO <sub>x</sub> /CsSn <sub>0.4</sub> Pb <sub>0.6</sub> I <sub>3</sub> /PCBM/BCP/Ag	0.87	25.74	74.6	16.79	2023 <sup>12</sup>
FTO/PEDOT:PSS/CsSn <sub>0.4</sub> Pb <sub>0.6</sub> I <sub>3</sub> / PCBM/BCP/Ag	0.88	26.29	71.83	16.62	2024 <sup>13</sup>
ITO/NiO <sub>x</sub> /Cs <sub>0.2</sub> FA <sub>0.8</sub> Sn <sub>0.4</sub> Pb <sub>0.6</sub> I <sub>3-x</sub> Br <sub>x</sub> / PCBM/ZrAcac/Ag	0.84	30.8	78.2	20.3	2025 <sup>14</sup>
ITO/DB-PTZPA/FA <sub>0.7</sub> MA <sub>0.3</sub> Sn <sub>0.4</sub> Pb <sub>0.6</sub> I <sub>3</sub> / EDA <sub>2</sub> /PCBM/C <sub>60</sub> /BCP/Ag	0.859	33.36	79.33	22.73	This work

**Table S2.** The detail data of forward and reverse sweep  $J$ - $V$  curve of PSCs with PEDOT:PSS, PTZPA and DB-PTZPA substrate.

	$V_{oc}$ (V)	$FF$ (%)	PCE (%)	$J_{sc}$ (mA cm <sup>-2</sup> )
<b>PEDOT: PSS(R)</b>	<b>0.801</b>	<b>76.65</b>	<b>20.11</b>	<b>32.75</b>
<b>PEDOT: PSS(F)</b>	<b>0.797</b>	<b>74.31</b>	<b>19.22</b>	<b>32.46</b>
<b>PTZPA(R)</b>	<b>0.819</b>	<b>77.69</b>	<b>21.07</b>	<b>33.11</b>
<b>PTZPA(F)</b>	<b>0.816</b>	<b>76.32</b>	<b>20.43</b>	<b>32.81</b>
<b>DB-PTZPA(R)</b>	<b>0.859</b>	<b>79.33</b>	<b>22.73</b>	<b>33.36</b>
<b>DB-PTZPA(F)</b>	<b>0.854</b>	<b>78.17</b>	<b>22.21</b>	<b>33.27</b>

**Table S3.** Fitting parameters of PSCs based on PEDOT:PSS, PTZPA and DB-PTZPA from Nyquist plots.

	$R_S(\Omega)$	$R_{REC}(\Omega)$
<b>PEDOT:PSS</b>	<b>32.5</b>	<b>985</b>
<b>PTZPA</b>	<b>26.3</b>	<b>1305</b>
<b>DB-PTZPA</b>	<b>12.4</b>	<b>1875</b>

## References

1. B. Zhao, M. Abdi-Jalebi, M. Tabachnyk, H. Glass, V. S. Kamboj, W. Nie, A. J. Pearson, Y. Puttison, K. C. Gödel, H. E. Beere, D. A. Ritchie, A. D. Mohite, S. E. Dutton, R. H. Friend and A. Sadhanala, *Adv. Mater.*, 2017, **29**, 1604744.
2. D. Ramirez, K. Schutt, Z. Wang, A. J. Pearson, E. Ruggeri, H. J. Snaith, S. D. Stranks and F. Jaramillo, *ACS Energy Lett.*, 2018, **3**, 2246-2251.
3. R. Prasanna, T. Leijtens, S. P. Dunfield, J. A. Raiford, E. J. Wolf, S. A. Swifter, J. Werner, G. E. Eperon, C. de Paula, A. F. Palmstrom, C. C. Boyd, M. F. A. M. van Hest, S. F. Bent, G. Teeter, J. J. Berry and M. D. McGehee, *Nat. Energy*, 2019, **4**, 939-947.
4. Z. Zhu, N. Li, D. Zhao, L. Wang and A. K. Y. Jen, *Adv. Energy Mater.*, 2019, **9**, 1802774.
5. S. A. Moyez, S. Maitra, K. Mukherjee, A. Sengupta and S. Roy, *J. Electron. Mater.*, 2020, **49**, 7133-7143.
6. M. T. Klug, R. L. Milot, J. B. Patel, T. Green, H. C. Sansom, M. D. Farrar, A. J. Ramadan, S. Martani, Z. Wang, B. Wenger, J. M. Ball, L. Langshaw, A. Petrozza, M. B. Johnston, L. M. Herz and H. J. Snaith, *Energy Environ. Sci.*, 2020, **13**, 1776-1787.
7. M. Hu, M. Chen, P. Guo, H. Zhou, J. Deng, Y. Yao, Y. Jiang, J. Gong, Z. Dai, Y. Zhou, F. Qian, X. Chong, J. Feng, R. D. Schaller, K. Zhu, N. P. Padture and Y. Zhou, *Nat. Commun.*, 2020, **11**, 151.
8. Q. Wen, C. Duan, F. Zou, D. Luo, J. Li, Z. Liu, J. Wang and K. Yan, *Chem. Eng. J.*, 2023, **452**, 139697.
9. M. Hu, G. Wang, Q. Zhang, J. Gong, Z. Xing, J. Gao, J. Wang, P. Zeng, S. Zheng, M. Liu, Y. Zhou and S. Yang, *J. Energy Chem.*, 2022, **72**, 487-494.
10. H. Guo, H. Zhang, S. Liu, D. Zhang, Y. Wu and W.-H. Zhu, *ACS Appl. Mater. Interfaces*, 2022, **14**, 6852-6858.
11. Z. Zhang, J. Liang, J. Wang, Y. Zheng, X. Wu, C. Tian, A. Sun, Z. Chen and C.-C. Chen, *Nano-Micro Lett.*, 2022, **14**, 165.
12. M. Hu, Y. Zhang, J. Gong, H. Zhou, X. Huang, M. Liu, Y. Zhou and S. Yang, *ACS Energy Lett.*, 2023, **8**, 1035-1041.
13. S. Chang, Z. Zhang, Y. Su, S. Yao, Y. Yang, Z. Yang, A. Wang, J. Cao, W. Huang, J. Dong and T. Qin, *Chem. Eng. J.*, 2024, **500**, 156707.
14. W. Zhang, H. Liu, T. Huang, L. Kang, J. Ge, H. Li, X. Zhou, W. Zhang, T. Shi and H.-L. Wang, *Adv. Mater.*, 2025, **37**, 2414125.